ELSEVIER

Contents lists available at ScienceDirect

Composites Part B

journal homepage: www.elsevier.com/locate/compositesb



Viscoelastic damping in crystalline composites: A molecular dynamics study



Raghavan Ranganathan*, Rahmi Ozisik, Pawel Keblinski

Department of Materials Science and Engineering, Rensselaer Polytechnic Institute, Troy, NY, 12180, USA

ARTICLE INFO

Article history:
Received 10 December 2015
Received in revised form
27 February 2016
Accepted 13 March 2016
Available online 19 March 2016

Keywords: Viscoelastic damping Crystalline nano-composites B. Mechanical properties C. Computational modeling

ABSTRACT

Molecular dynamics (MD) simulations were used to study viscoelastic behavior of model Lennard-Jones (LJ) crystalline composites subject to an oscillatory shear deformation. The two crystals, namely a soft and a stiff phase, individually show highly elastic behavior and very small loss modulus. On the other hand, when the stiff phase is included within the soft matrix as a sphere, the composite exhibits significant viscous damping and a large phase shift between stress and strain. In fact, the maximum loss modulus in these model composites was found to be about 20 times greater than that given by the theoretical Hashin-Shtrikman upper bound. We attribute this behavior to the fact that in composites shear strain is highly inhomogeneous and mostly accommodated by the soft phase. This is corroborated by mode-dependent Grüneisen parameter analysis showing that in the low frequency regime, Grüneisen parameters, which measure degree of anharmonicity, are about twice greater for the composite than each individual homogenous crystal. Interestingly, the frequency at which the damping is greatest scales with the microstructural length scale of the composite, a feature we also observe for superlattice structures.

© 2016 Elsevier Ltd. All rights reserved.

1. Introduction

Versatility in tuning viscoelastic properties from a purely viscous to a purely elastic behavior has enabled a wide range of engineering applications such as artificial tissues [1], functional foams [2], optoelectronics [3] among a slew of structural and mechanical applications [4]. Viscoelasticity can be exploited to synthesize materials with exceptional damping properties. Notably, polymer composites have been designed for damping and noise reduction in automobiles and airplanes [5], conferring structural stability during wind and earthquake induced vibrations [6], and mechanical damping in a number of applications [7–11]. There exists a large body of work on experimental characterization of damping and its dependence on various variables like temperature, microstructure and shear deformation frequency for polymer and fiber composites [10,12–15].

Recently, viscoelasticity in crystalline materials such as metals and alloys has garnered a lot of attention. The main promise of these materials is to maintain high stiffness (high elastic modulus)

E-mail addresses: rangar2@rpi.edu (R. Ranganathan), keblip@rpi.edu (P. Keblinski).

while providing significant damping, i.e., relatively high loss modulus. For example, Ma et al. [16] studied the composition dependence of aluminum in AlCoCrFeNi high entropy alloys and showed that increasing aluminum content significantly increased damping. Schaller [11] studied the loss behavior in Mg—Si metal matrix composites and observed large viscous damping arising from successive pinning and unpinning of dislocations during cyclic shear loading. Muthusamy et al. [17] reported exceptional damping properties in cement-matrix graphite network composite with the loss factor approaching 0.8. Srikanth et al. [18] showed that by progressively adding more and more copper to a magnesium alloy, the damping capacity could be enhanced by about 100%.

Ferroelectrics are another class of materials that demonstrate high loss moduli arising from switching of domains in the presence of oscillating electric fields [19]. It has also been shown that presence of a negative stiffness phase (those that are pre-constrained by residual forces) in composites can give rise to very high damping [20–22] with a loss factor on the order of 1–4. However, these materials require a positive stiffness phase to maintain mechanical integrity.

A large body of theoretical work in predicting bounds for elastic and shear moduli for materials has been performed over the years. These are either based on the well-known variational theory

^{*} Corresponding author.

propounded by Hashin and Shtrikman [23,24]; continuum based methods [25–27] or multiscale modeling [28]. Also popular are techniques that couple homogenization theory to obtain bounds for material properties and a structural optimization algorithm to model microstructures with tunable properties [29]. While these methods are valuable predictive tools for estimating composite viscoelastic properties, a deeper understanding of the underlying mechanisms is possible only using molecular level simulations. Molecular Dynamics (MD) lends itself as a powerful tool for understanding and predicting viscoelastic properties of a wide variety of materials including polymer melts [30], crosslinked rubber composites [31].

In the current work, we use non-equilibrium Molecular Dynamics shear simulations to study viscoelasticity of model crystalline composites with various microstructures as a function of shear rate. We limit ourselves to deformations where there are no defects such as dislocations formed, thus, the damping is obtained purely due to the anharmonic coupling between vibrational modes.

2. Simulation methodology

The simulation methodology involves application of an oscillatory shear deformation at a range of frequencies (shear rates) to crystalline composite microstructures. We evaluate the loss and storage moduli directly from the time dependent stress-strain data.

2.1. Model composite structures

Our model composites are comprised of a "stiff" spherical inclusions inside a "soft" matrix. Both phases are crystalline, in a face centered cubic (FCC) lattice, and are modeled by the standard 12-6 Lennard Jones potential:

$$E = 4\varepsilon \left[\left(\frac{\sigma}{r} \right)^{12} - \left(\frac{\sigma}{r} \right)^{6} \right] \tag{1}$$

where ε and σ for the soft phase are equal to 0.01 eV and 3.405 Å, respectively. These values correspond to those of FCC crystal of argon [32]. The ε for the stiff phase is increased by four times that of the soft phase. The σ values are the same for both soft and stiff crystals rendering the interface between them epitaxial and resulting in very low residual stresses. A common cutoff of 10 Å is used for truncating the potential interaction. Atomistic snapshots of a homogeneous soft phase, a composite with a stiff inclusion of volume fraction (ϕ) of 0.4, and a homogeneous stiff phase are shown in Fig. 1 (panels (a), (b) and (c), respectively). All three cases comprised of 25 unit cells in a FCC lattice in each dimension (62500 atoms in total) with a cubic simulation cell size of ~133 Å.

2.2. Application of non-equilibrium oscillatory shear

Viscoelastic properties are studied using non-equilibrium oscillatory shear deformation simulations. We apply a homogeneous, sinusoidal shear strain, γ_{xy} , with a shear frequency (f) to the cubic simulation cell as described in Eq. (2):

$$\gamma_{xy} = \gamma_0 \sin(2\pi f t) \tag{2}$$

where γ_{xy} refers to strain applied within the xz-plane along the x-axis in a right-handed coordinate system, γ_o is the maximum shear strain imposed on the system. Using the molecular-level virial formula [33], we then calculate the resulting shear stress, τ_{xy} . Note that during this shear deformation, the simulation box volume remains constant while the shape of the simulation cell changes due to the applied shear strain.

One expects τ_{xy} to follow the same sinusoidal profile as γ_{xy} and this is indeed seen to be the case in all our simulations. Therefore, the shear stress can be described by a sinusoidal function having a phase shift angle (δ) as described in Eq. (3):

$$\tau_{xy} = \tau_0 \sin(2\pi f t + \delta) \tag{3}$$

The phase angle (δ) is a measure of the viscoelasticity of the material. Purely elastic materials have $\delta=0^\circ$ and purely viscous materials have $\delta=90^\circ$. In the current simulations, we accumulate τ_{xy} over multiple shear cycles to calculate the shear modulus (G), which is defined as the ratio of the maximum shear stress $(\tau_{xy, max})$ and the maximum shear strain $(\gamma_{xy, max})$. The shear modulus is a complex quantity that is usually expressed as the complex sum of the storage $(G'=G\cos(\delta))$ and loss $(G''=G\sin(\delta))$ moduli.

$$G = \frac{\tau_{xy,max}}{\gamma_{xy,max}} = G\cos(\delta) + iG\sin(\delta)$$
 (4)

Estimation of viscoelasticity from averaged stress-strain curves during oscillatory shear deformation is depicted in Fig. 1. The oscillatory shear strain (γ_{xy}) imposed on the system is shown in blue and the resulting shear stress (τ_{xy}) is shown in green. The stress-strain data are averaged over 40 shear cycles and the time period of oscillations is 5 ps $(f=0.2~{\rm ps}^{-1})$. Panels (a), (b) and (c) in Fig. 1 correspond to results obtained from homogeneous soft, composite with $\phi\sim0.4$ and, homogeneous stiff phase, respectively. The phase angle (δ) between stress and strain and the magnitude of shear modulus are also shown for all three cases. We observe that for homogeneous phases (both soft and stiff), δ is close to zero, resulting in a negligible loss modulus. On the other hand, the composite microstructure shows a large δ (~22°) leading to significant loss modulus.

For all shear simulations, we first equilibrate the system at 40 K and zero pressure using a Nose-Hoover thermostat [34.35] for 400 ps. The damping time constants for the thermostat and barostat are 100 fs and 200 fs, respectively. This is followed by further equilibration at constant volume and constant temperature (NVT) ensemble for 400 ps. The equilibrated structures are then subjected to the oscillatory shear simulations at constant volume and constant energy (NVE) ensemble to characterize viscoelasticity. The thermostat is removed during shear in order not to artificially remove heat dissipated during shearing. Additionally, this allows us to monitor the rise in the system temperature (and energy) during shear, and thus, we ensure that the shear cycles are terminated well below the melting point of the soft phase (84 K) [36]. We note that the crystallinity of the composite is maintained during both equilibration and cyclic shear deformation stages, which were confirmed by negligible variation in the pair distribution function between the relaxed and strained structures and the coordination of all atoms, which was found to be equal to 12 (FCC). For all simulations, the stress profiles were averaged over 3 to 5 cycles, ensuring that the system temperature does not exceed ~45 K. The simulation box size (L) ranged from 7 unit cells (~37 Å) to 25 unit cells (~133 Å) and the maximum shear strain imposed was within 1.5%. All simulations were performed with the LAMMPS simulation package [37] with a timestep of 2 fs. Periodic boundary conditions were applied along all three axes.

3. Results and discussion

In this section, we describe the characteristics of viscoelastic behavior of composites under oscillatory shear. Section 3.1 elucidates the primary explanation of high viscous losses in these materials by means of vibrational property characteristics of the composite. The effects of microstructure, composition of the phases

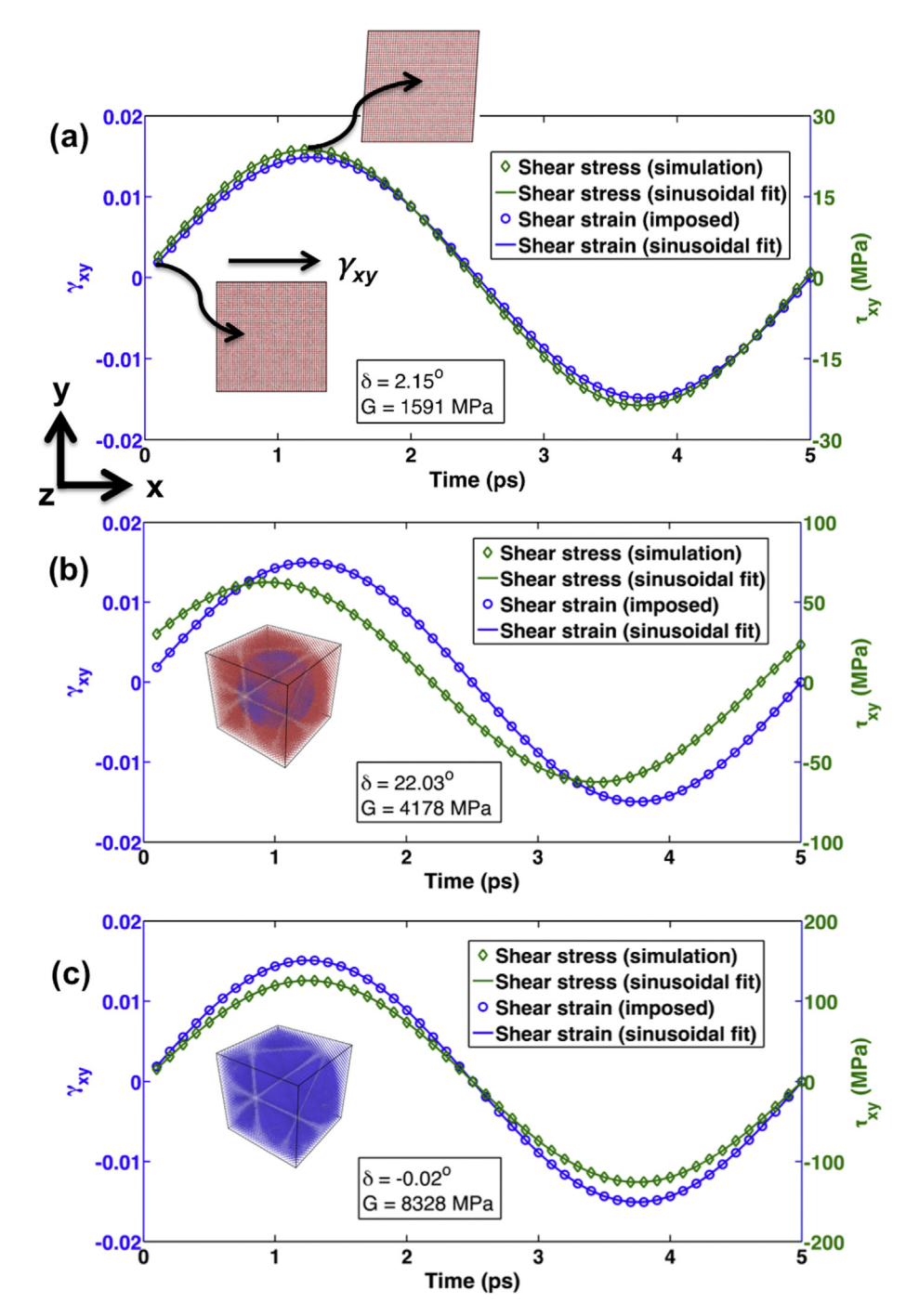


Fig. 1. Estimation of viscoelasticity from averaged stress-strain curves during oscillatory shear deformation. Shear strain (γ_{xy}) is the input and shear stress (τ_{xy}) is the output. Panels (a) and (c) are for homogeneous soft and stiff phases respectively that exhibit negligible phase difference. Panel (b) is for a composite with the volume fraction of stiff phase $\varphi \sim 0.4$ exhibiting significant phase shift and thus, a large loss modulus. Side views in panel (a) show the zero-strain and maximum strain configurations during the shear cycle.

and shear frequency on viscous damping are presented in Section 3.2. Finally, we extend our analysis to superlattice structures composed of soft and stiff phases (Section 3.3).

3.1. Vibrational analysis

The viscoelastic properties of a material are likely to be dictated by its vibrational properties in our simulations, as no defect formation or bond breaking are observed. During the oscillatory shear deformation, the energy dissipation occurs via the anharmonic coupling between the various phonon modes. The degree of anharmonic coupling between the phonon modes determines the extent of viscoelastic loss in such material. A direct measure of this is the mode-dependent Grüneisen parameter, γ [38], defined by Eq. (5). γ relates the shift in individual phonon frequencies (ω_i) to infinitesimal changes in system volume, V.

$$\gamma_i = -\frac{V}{\omega_i} \frac{\partial \omega_i}{\partial V} \tag{5}$$

where γ_i is the Grüneisen parameter of the ith phonon mode. A larger γ implies greater energy dissipation (loss) due to larger anharmonic coupling.

We calculate γ for all the system frequencies using Eq. (5) upon deforming the simulation cell isotropically, during which the volume is changed by 1% about the equilibrium volume. For each volume, the phonon frequencies and were calculated by the diagonalization of a dynamical matrix [39] using the Xenoview software package [40].

Shown in Fig. 2 is the variation of γ_i for various composites ranging from $\phi = 0$ (fully soft) to $\phi = 1$ (fully stiff) for L = 7 unit cells. The homogeneous soft phase ($\phi = 0$) shows a maximum γ of about 8 at the low frequency end (~0.2 THz). The pure stiff phase ($\phi = 1$), has a maximum γ of about 5. The two intermediate volume fractions ($\phi = 0.27$ and $\phi = 0.47$) exhibit much larger γ (for example, at $\phi = 0.47$, ~2 and ~3 times larger than homogeneous soft and stiff phases, respectively), which is due to a large strain concentration in narrow regions of the soft phase. In fact, the soft phase is seen to experience a much larger shear strain (2-10 times greater) compared to the stiff phase and it increases monotonically with radial distance with the least strain present at the epitaxial interface (refer to Section S1 and Figure S1 in supplementary information for a detailed analysis on local strain distribution analysis). Confinement of a softer phase in a composite can thus potentially result in significant viscous damping via large local deformation.

3.2. Role of composite microstructure and shear frequency on damping

Viscous damping in materials is a complex phenomenon that depends on various factors. Among the most important are the structure of the material (i.e., the microstructure of crystalline composites) and the shear frequency. In this section, we study the effect of two important contributors to viscoelastic damping in composites, namely, the composite microstructure and shear frequency. The microstructural effect is studied in two ways. First, we fix the overall simulation cell size and vary the volume fraction of the stiff inclusion (denoted as "volume-fraction-sweep"). We then study the effect of shear frequency (denoted as "frequency-sweep") for various microstructural features. Here, the second kind of microstructural effect is realized by keeping the volume fraction of the spherical inclusion fixed while varying the overall simulation cell size. Coupled with this are possible size effects that are also addressed.

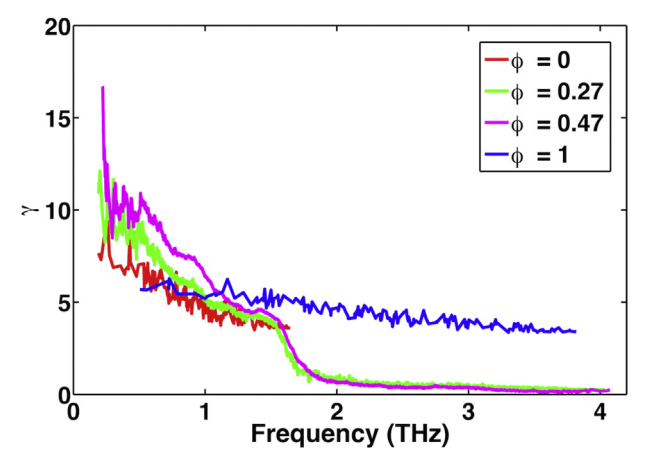


Fig. 2. Variation of mode-dependent Grüneisen parameters for various composites, ranging from $\varphi = 0$ (fully soft) to $\varphi = 1$ (fully stiff) for a system size of L = 7 unit cells.

At the nanoscale, microstructure is expected to play a huge role in damping due to a large interfacial effect. To understand the effect of microstructure on damping properties of crystalline composites, various simulations were performed where the volume fraction of the stiff phase (ϕ) is varied from 0 to 1 ("volume-fraction-sweep") while keeping the shear rate constant. It is also well known that viscous damping in materials is strongly affected by the shear rate [41]. At high shear rates, materials cannot respond to high rate of deformation, and consequently, behaves like a glass with a high storage modulus and low viscous loss. In the low frequency regime, there is sufficient time for material to respond to shear deformation, which leads to elastic-like behavior and low viscous losses.

3.2.1. The effect of inclusion volume fraction

We study a range of microstructures by varying the volume fraction (ϕ) of the stiff inclusion. Shown in Fig. 3 are the results for volume-fraction-sweep simulations for a fixed simulation box size of L=7 and at a constant shear frequency of 0.33 THz. Two possible arrangements of component phases were considered: (a) the inclusion being the stiff phase (shown by red circles) and (b) the inclusion being the soft phase (shown by green triangles). We observe that the loss modulus is close to zero for homogeneous compositions ($\phi = 0$ and $\phi = 1$). At intermediate fractions of the stiff phase (0.2 < ϕ_{stiff} < 0.6), there is significant viscoelastic damping and the maximum loss modulus of ~1500 MPa is approximately 25 times larger than that of the homogeneous soft phase. The loss modulus profiles of the two cases (soft versus stiff inclusion) are somewhat different - the stiff inclusion case shows slightly enhanced damping. We suppose that this is due to the soft matrix experiencing the majority of the deformation and not transferring much of the deformation to the stiff inclusion. We note that the observed enhancements in loss moduli for composites are about 20 times greater than the analytical upper bounds predicted by the Hashin-Shtrikman variational theory [24]. This theory assumes homogeneous deformation of component phases in a composite, and as a consequence, predicts the composite moduli bound by the inherent moduli of the component phases. In our model composites however, the selective deformation of the soft phase along with large Grüneisen parameters (as discussed in Section 3.1) is responsible for this enhanced damping. Details about this comparison with the Hashin-Shtrikman theory is presented in supplementary information and is depicted in Figure S2).

The stiffness of the inclusion phase should have a significant effect on damping; the bigger the contrast between the phases, the

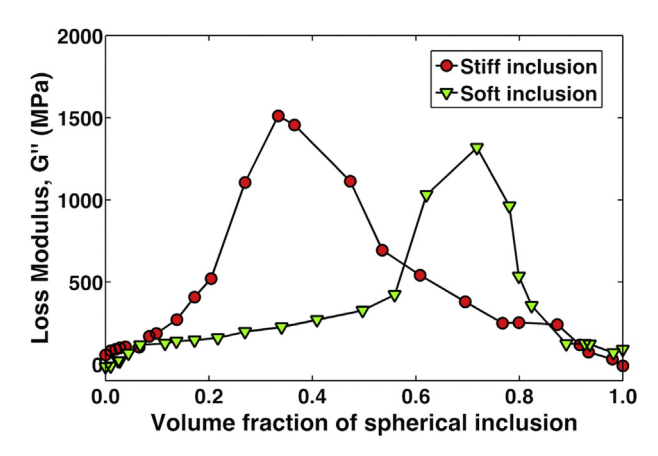


Fig. 3. *Volume-fraction-sweep* simulations showing variation of loss modulus as a function of volume fraction of the spherical inclusion. The two sets of data represent the arrangement of the phases (the inclusion being either soft or stiff). The shear frequency is fixed at 0.33 THz.

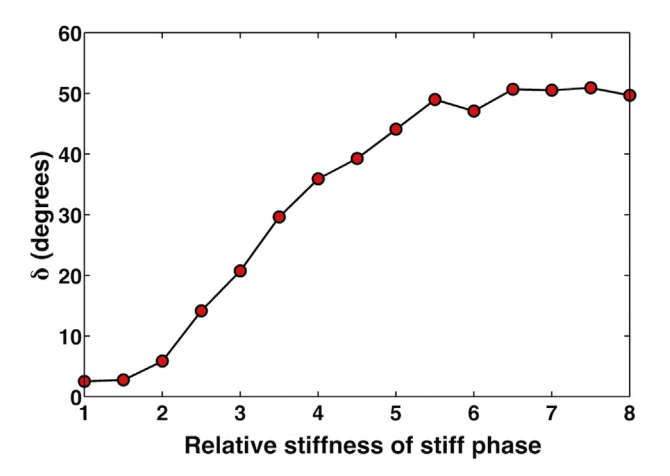


Fig. 4. Variation of loss modulus with stiffness of the stiff phase. The relative stiffness is represented as the ratio of ε_{soft} .

greater is the strain accommodated by the softer phase (the matrix). This is clearly seen in our simulations and is depicted in Fig. 4 for a composite with $\phi=0.5$ and L=7 at a shear frequency of 0.4 THz, which corresponds to the frequency of maximum loss modulus for this system. The relative stiffness (ε_{rel}) is represented as the ratio of ε_{stiff} to ε_{soft} . For a relative stiffness of one (homogeneous soft phase), we recover the negligible damping behavior of the homogeneous soft phase noted earlier in Fig. 3. Loss modulus increases almost linearly with relative stiffness in the ε_{rel} range of 2–4 and begins to saturate for $\varepsilon_{rel} > 5$.

3.2.2. The effects of microstructure and simulation cell size

In this section, we first consider the possible size effect from the choice of simulation cell size on damping. *Frequency-sweep* simulations were performed for a composite with $\phi = 0.5$ for three

different structures. The first structure comprises of a single spherical inclusion with L = 7 unit cells. The other two structures are obtained by replicating the base structure (L = 7) two and three times in each axis to yield structures with L=14 and L=21 unit cells. These structures have eight and twenty-seven times the volume (and also number of inclusions) of the base structure respectively. Thus, here we merely study the effect of simulation cell size on damping, while preserving the same microstructure in all three structures. Shown in Fig. 5 are the results of the frequencysweep simulations for the three microstructures, with the maximum shear strain fixed at 1.5% for all cases. As seen from the figure, at either end of the shear frequency spectrum (low frequency end at $f \sim 0.01$ THz and the high frequency end at $f \sim 2$ THz), the loss modulus is negligibly small. At intermediate frequencies (0.3 < f < 1.5 THz), a large loss modulus results. This is because, at low frequencies, the system has ample time for the shear stress to respond to the strain. On the other hand, at high frequencies, the system is forced to follow the extremely fast deformation, akin to a glassy behavior. For either case, the phase angle is close to zero. At intermediate shear frequencies that correspond to high Grüneisen parameters (refer to Fig. 2), we observe significant damping, with the peak modulus value typically two orders of magnitude greater than that observed at the lowest frequency (0.01 THz). Thus, damping is greatly enhanced for composites near shear frequencies that correspond to the vibrational frequencies of the composite. Since we observe almost identical results for all three cases (which have identical microstructures), we conclude that there are no artifacts from the choice of the simulation cell size used in this work.

Next, we explore the microstructural size effect by varying the simulation cell size while keeping the volume fraction of the stiff phase (ϕ) is fixed. Shown in Fig. 6 (a) are the results of the *frequency-sweep* simulations depicting the variation of loss modulus with frequency for various system sizes containing L=7, 10, 14, 20 and 25 unit cells in each direction at $\phi=0.48$. The maximum shear strain is fixed at 1.5% for all cases. The homogeneous phases (soft,

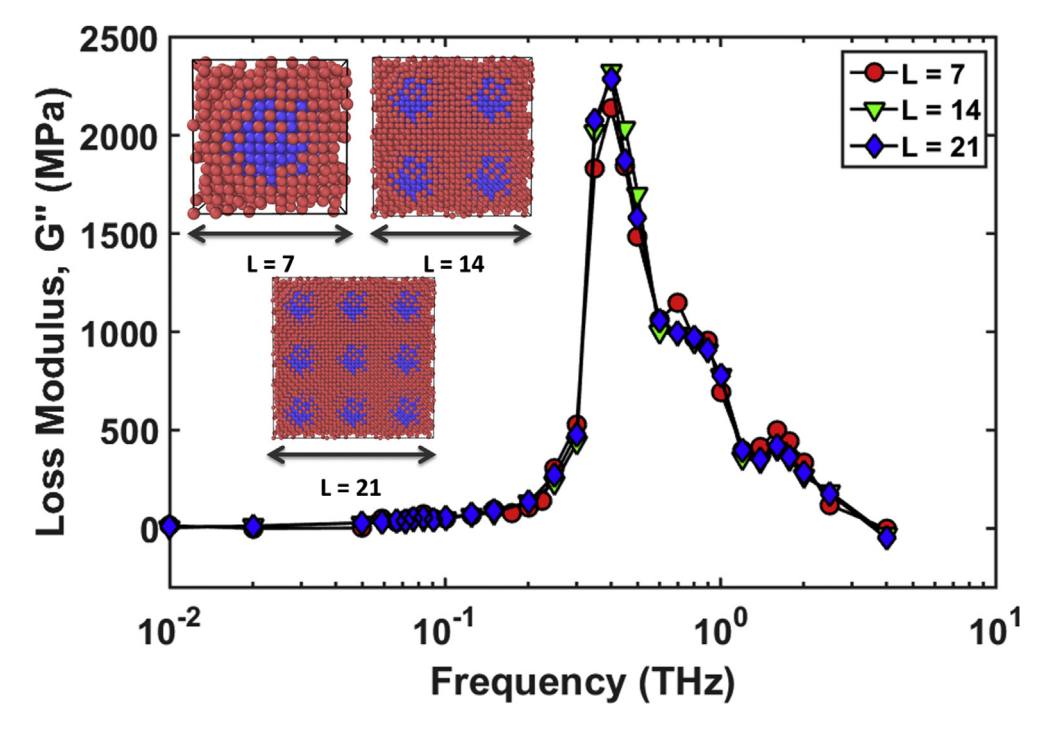


Fig. 5. Frequency-sweep simulations for composite with volume fraction of stiff phase, $\varphi \sim 0.5$ for the base composite of size L=7 unit cells (red circles) and the base structure replicated twice (L=14 unit cells) and thrice (L=21 unit cells) along x, y and z axes (green triangles). The atomic snapshots for these structures are shown as insets. (For interpretation of the references to colour in this figure legend, the reader is referred to the web version of this article.)

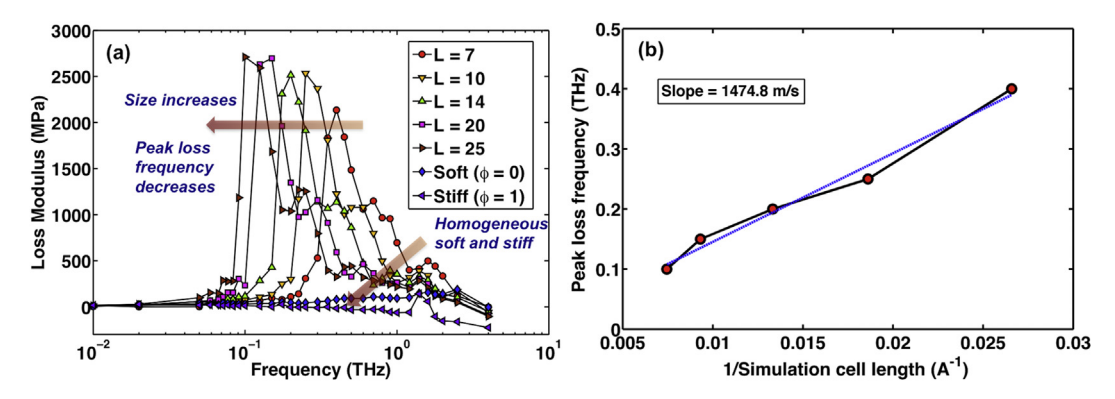


Fig. 6. (a) *Frequency-sweep simulations* depicting variation of loss modulus with frequency for various system sizes from L=7 unit cells to L=25 unit cells, with the volume fraction of stiff phase, $\varphi \sim 0.48$. The homogeneous phases ($\varphi = 0$ and $\varphi = 1$) which exhibit negligible loss moduli are also shown for comparison. (b) Variation of peak loss frequency with inverse of simulation cell length as outlined in panel (a).

 $\phi = 0$; and stiff, $\phi = 1$), which exhibit negligible loss moduli at all frequencies, are also shown for comparison. As seen from the figure, increasing system size results in the maximum G'' versus frequency curve to shift to lower frequency. Interestingly, the peak loss frequency, when plotted against the inverse of simulation cell length gives rise to a straight line with a positive slope of about 1475 m/s as shown in Fig. 6 (b). This value should be related to the speed of sound wave (c') due to propagation of shear waves in the composite. The speed of sound due to shear in the composite with $\phi = 0.48$ was also computed from MD determined elastic properties using the relation $c = \sqrt{G/\rho}$ [42] was found to be 1270.1 m/s. The similar values of the speed of sound and the slope calculated from maximum damping frequency versus inverse size suggests that the maximum damping corresponds approximately to the frequency of the largest wavelength sound wave representing microstructure periodicity.

3.3. Viscoelasticity in crystalline superlattice structures

Superlattice or laminated structures, where usually two dissimilar materials with different mechanical properties are sandwiched together, lead to many interesting properties [43]. Skirlo et al. [44] studied viscoelasticity in model Cu—Nb superlattice structures with stepped interfaces and found that the interfacial shear modulus increases monotonically with the step density. With this motivation, we also explore damping in superlattice with layers of the two components (soft and stiff) having the same thickness ($\phi=0.5$). Akin to our analysis with regards to the size and shear frequency effects on damping in spherical inclusion

composites, we observe that superlattice structures exhibit a similar damping behavior. Fig. 7 (a) shows the frequency-sweep simulations for superlattice structures with varying sizes, plotted as a function of superlattice period. The sizes are such that the period of the superlattice feature (width of one layer of soft and stiff phase) is varied from L = 4 unit cells (10.8 Å) to L = 24 unit cells (64.5 Å). A snapshot of the superlattice structure with a period of 8 unit cells (21.5 Å) is shown in the inset. As observed for the spherical inclusion composites, superlattice structures are also observed to exhibit high loss moduli at intermediate frequencies. Interestingly, we observe two pronounced peaks in the loss moduli for all sizes. We denote these as the "high-frequency" and "low-frequency" peaks just based on the frequency position. Two trends are clearly evident with respect to this characteristic damping. Firstly, as the superlattice period decreases, the low-frequency peak intensity decreases and the high-frequency peak increases. For the smallest structure (with a period of 4 unit cells), the low-frequency peak appears as a mere shoulder. This clearly shows that the lowfrequency peak originates from the layering in superlattice, which disappears as the superlattice period diminishes (becomes more homogeneous). We suppose this is because of greater strains undergone by the soft phase when the superlattice period increases.

Secondly, one can observe the characteristic size-dependence for damping, in that larger sizes shift the damping frequencies to lower values. We observe that both the high- and low-frequency peaks show this behavior. Fig. 7 (b) shows the variation of these two peak frequencies as a function of inverse superlattice width. We observe that the high-frequency peak has a slope of 3533.8 m/s, which is about 1.4 times larger than that for the low-frequency

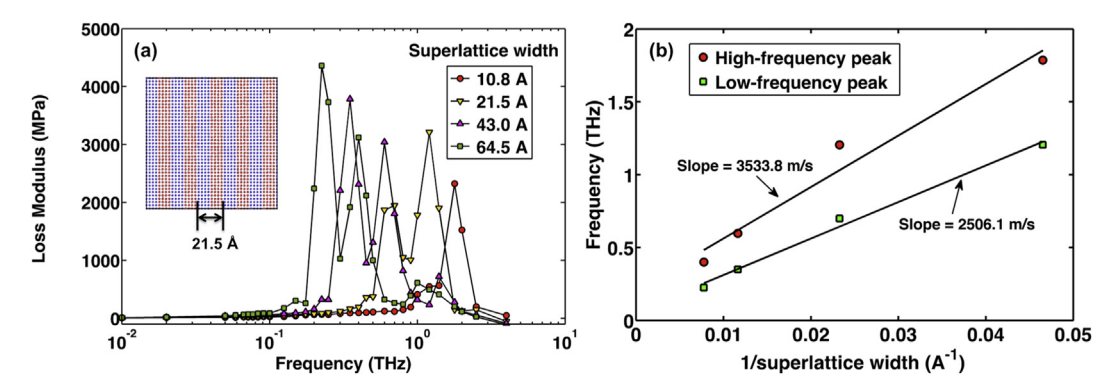


Fig. 7. (a) *Frequency-sweep simulations* for superlattice structures composed of soft and stiff phases, for various widths of the superlattice spacing. (b) Variation of the two peak loss frequencies (the high and low-frequency peaks) as obtained in panel (a), with inverse of superlattice width.

peak. It is possible that the two peaks relate to longitudinal and transverse vibrational modes characterized by the difference in speed of sound.

4. Conclusions

Using non-equilibrium molecular dynamics shear simulations, we demonstrate high viscoelastic damping (manifested as large loss modulus, G'') in model crystalline composites with spherical inclusion of a stiff phase embedded in a softer matrix. These high losses are realized only for intermediate volume fractions (ϕ) of the stiff phase (0.2 < ϕ _{stiff} < 0.6) and at intermediate shear frequencies (0.3 < f < 1.5 THz) which are seen to overlap with the range of system frequencies present. In summary, we find that:

- 1. Viscoelastic damping has a strong dependence on the microstructure of the composite with homogeneous phases (purely soft or purely stiff), exhibiting negligibly small loss moduli and intermediate volume fractions of the stiff phase exhibiting up to 25 times larger loss moduli than the homogeneous soft phase.
- 2. Viscoelastic damping in composites exhibits a strong shear frequency dependence. At intermediate shear frequencies, the loss modulus can increase by about two orders of magnitude. Closely associated with this frequency-dependence is the sizedependence of loss moduli. We observe that for a fixed volume fraction of the stiff phase, larger simulation cell lengths result in a linear reduction of frequency at which the peak loss modulus occurs.
- 3. We attribute the large loss moduli in composites to selectively large deformation of the soft phase. At intermediate volume fractions of the stiff phase, we observe confinement of large shear strains in the soft phase, resulting in mode-dependent Grüneisen parameters that are 2–3 times larger than for homogenous soft and stiff phases respectively. The loss moduli can be up to 20 times larger than analytical upper bounds predicted by the variational theory of Hashin and Shtrikman.
- 4. We also observe high viscoelastic losses in model superlattice structures comprising of soft and stiff crystalline components that are dependent on the shear frequency and the superlattice width. In particular, we observe two peaks in the loss moduli during *frequency-sweep* simulations, with the low-frequency peak corresponding to the superlattice feature that diminishes as the superlattice width decreases (becomes more homogenous).

Appendix A. Supplementary data

Supplementary data related to this article can be found at http://dx.doi.org/10.1016/j.compositesb.2016.03.037.

References

- Tang Z, Kotov NA, Magonov S, Ozturk B. Nanostructured artificial nacre. Nat Mater 2003;2:413–8.
- [2] Lee LJ, Zeng C, Cao X, Han X, Shen J, Xu G. Polymer nanocomposite foams. Compos Sci Technol 2005;65:2344–63.
- [3] Mitra S, Cook S, Švrček V, Blackley RA, Zhou W, Kovač J, et al. Improved optoelectronic properties of silicon nanocrystals/polymer nanocomposites by microplasma-induced liquid chemistry. J Phys Chem C 2013;117:23198–207.
- [4] Lakes RS. Viscoelastic materials. ed. 1. New York: Cambridge Univ. Press; 2009.
- [5] Rao MD. Recent applications of viscoelastic damping for noise control in automobiles and commercial airplanes. J Sound Vib 2003;262:457–74.
- [6] Samali B, Kwok KCS. Use of viscoelastic dampers in reducing wind- and earthquake-induced motion of building structures. Eng Struct 1995;17: 639–54.

- [7] Jung WY, Aref AJ. A combined honeycomb and solid viscoelastic material for structural damping applications. Mech Mater 2003;35:831–44.
- [8] Katiyar P, Kumar A. A study of damping characteristics of alumina-filled epoxy nano-composites. Proc SPIE 2013;8689:86891M. 8689.
- [9] Adams RD, Maheri MR. Damping in advanced polymer-matrix composites. | Alloys Compd 2003;355:126–30.
- [10] Chandra R, Singh SP, Gupta K. Damping studies in fiber-reinforced composites a review. Compos Struct 1999;46:41–51.
- [11] Schaller R. Metal matrix composites, a smart choice for high damping materials. | Alloys Compd 2003;355:131–5.
- [12] Benchekchou B, Coni M, Howarth HVC, White RG. Some aspects of vibration damping improvement in composite materials. Compos Part B Eng 1998;8368;809—17.
- [13] Treviso A, Van Genechten B, Mundo D, Tournour M. Damping in composite materials: properties and models. Compos Part B Eng 2015;78:144–52.
- [14] Sharafi S, Li G. Multiscale modeling of vibration damping response of shape memory polymer fibers. Compos Part B Eng 2016;91:306–14.
- [15] Feng J, Guo Z. Temperature-frequency-dependent mechanical properties model of epoxy resin and its composites. Compos Part B Eng 2016;85:161–9.
- [16] Ma SG, Liaw PK, Gao MC, Qiao JW, Wang ZH, Zhang Y. Damping behavior of AlxCoCrFeNi high-entropy alloys by a dynamic mechanical analyzer. J Alloys Compd 2014:604:331–9.
- [17] Muthusamy S, Wang S, Chung DDL. Unprecedented vibration damping with high values of loss modulus and loss tangent, exhibited by cement-matrix graphite network composite. Carbon 2010;48:1457–64.
- [18] Srikanth N, Gaofeng CH, Gupta M. Enhanced damping of a magnesium alloy by addition of copper. J Alloys Compd 2003;352:106–10.
- [19] Wojnar CS, le Graverend J-B, Kochmann DM. Broadband control of the viscoelasticity of ferroelectrics via domain switching. Appl Phys Lett 2014;105:162912.
- [20] Jaglinski T, Kochmann D, Stone D, Lakes RS. Composite materials with viscoelastic stiffness greater than diamond. Science 2007;315:620–2.
- [21] Lakes RS. Extreme damping in composite materials with a negative stiffness phase. Phys Rev Lett 2001;86:2897–900.
- [22] Lakes RS, Lee T, Bersie A, Wang YC. Extreme damping in composite materials with negative-stiffness inclusions. Nature 2001;410:565–7.
- [23] Hashin Z, Shtrikman S. A variational approach to the theory of the elastic behaviour of multiphase materials. J Mech Phys Solids 1963;11:127–40.
- [24] Hashin Z. Complex moduli of viscoelastic composites—I. General theory and application to particulate composites. Int J Solids Struct 1970;6:539—52.
- [25] Berthelot J-M, Assarar M, Sefrani Y, Mahi AE. Damping analysis of composite materials and structures. Compos Struct 2008;85:189–204.
- [26] Meaud J, Sain T, Hulbert GM, Waas AM. Analysis and optimal design of layered composites with high stiffness and high damping. Int J Solids Struct 2013;50: 1342–53.
- [27] Kim HJ, Swan CC, Lakes RS. Computational studies on high-stiffness, high-damping SiC-InSn particulate reinforced composites. Int J Solids Struct 2002;39:5799–812.
- [28] Attipou K, Nezamabadi S, Daya EM, Zahrouni H. A multiscale approach for the vibration analysis of heterogeneous materials: application to passive damping. J Sound Vib 2013;332:725–39.
- [29] Huang X, Zhou S, Sun G, Li G, Xie YM. Topology optimization for microstructures of viscoelastic composite materials. Comput Methods Appl Mech Eng 2015;283:503—16.
- [30] Sen S, Sen S, Kumar S, Kumar S, Keblinski P, Keblinski P. Viscoelastic properties of polymer melts from equilibrium molecular dynamics simulations. Macromolecules 2005;38:650–3.
- [31] Yagyu H, Utsumi T. Coarse-grained molecular dynamics simulation of nanofilled crosslinked rubber. Comput Mater Sci 2009;46:286–92.
- [32] Hansen J, Verlet L. Phase transition of the Lennard-Jones system. Phys Rev A 1969;184:151–61.
- [33] Thompson AP, Plimpton SJ, Mattson W. General formulation of pressure and stress tensor for arbitrary many-body interaction potentials under periodic boundary conditions. J Chem Phys 2009;131:1–6.
- [34] Nose S. A unified formulation of the constant temperature molecular dynamics methods. J Chem Phys 1984;81:511–9.
- [35] Hoover WG. Canonical dynamics: equilibrium phase-space distributions. Phys Rev A 1985;31:1695–7.
- [36] Nose S, Yonezawa F. Isothermal-isobaric computer simulations of melting and crystallization of a Lennard-Jones system. J Chem Phys 1986;84:1803—14.
- [37] Plimpton S. Fast parallel algorithms for short-range molecular dynamics. J Comput Phys 1995;117:1–19.
- [38] Gruneisen E. Handbook of physics. 1926.
- [39] Ashcroft NW, Mermin DN. Solid state physics. 1976.
- [40] Shenogin S, Ozisik R. See http://xenoview.mat.rpi.edu, 2007.
- [41] Painter PC, Coleman MM. Essentials of polymer science and engineering. 2008.
- [42] Krautkramer J, Krautkramer H. Ultrasonic testing of materials. 1990.
- [43] Stoloff NS, Davies RG. The mechanical properties of ordered alloys. Prog Mater Sci 1968;13:1–84.
- [44] Skirlo SA, Demkowicz MJ. Viscoelasticity of stepped interfaces. Appl Phys Lett 2013;103:171908.